

# Electrical Performance Estimations for Shaped Dielectric Lens Antenna with Array Feed

Yosuke Tajima, Shinji Kamada, Naobumi Michishita and Yoshihide Yamada

Department of Electrical and Electronic Engineering  
National Defense Academy  
1-10-20 Hashirimizu, Yokosuka-shi, 239-8686 JAPAN  
yyamada@nda.ac.jp

**Abstract**—A shaped dielectric lens antenna with simple array feeds was developed to realize wide-angle beam scanning in car-mounted radar systems. The electrical performance of the dielectric lens antenna has been previously studied through electromagnetic simulations. The authors fabricated a practical dielectric lens antenna operating at 20 GHz and measured its performance. A convenient patch antenna configuration was developed for the array feed. A power divider comprising eight branched microstrip lines was designed in order to achieve precise excitation coefficients for the array feed. Design accuracy of the array feed was confirmed from measured and calculated results for the excitation coefficients and radiated electric field. To determine the wide-angle beam scanning characteristics, the aperture amplitude and phase distributions were estimated numerically using the obtained array radiated electric field. Excellent flat-phase characteristics were confirmed. The commercial electromagnetic simulator FEKO was employed for the numerical simulations. The radiation patterns at a 30° beam scanning angle were measured. Very good agreements between the measured and calculated results were found. Moreover, sufficient antenna gain was confirmed through experiments.

**Index Terms**— Shaped dielectric lens antenna, array feed, wide-angle beam scanning, electromagnetic simulation.

## I. INTRODUCTION

Communication and car safety systems are under development as part of the Intelligent Transportation Systems (ITS) operating in the millimeter-wave frequency bands [1, 2]. For collision avoidance, car radar systems that can scan 15° have been developed. However, in order

to expand the system for local street use, wide-angle beam scanning ability of over 30° is necessary. For this, a dielectric lens antenna is considered one of the promising candidates [3]. The authors have been studying shaped dielectric lens antennas. Lens shaping based on Abbe's sine condition [4] was proven to have excellent wide-angle beam scanning capability [5]. Moreover, the wide-angle beam scanning capability can be further improved by employing simple array feeds [6]. Previously, the electrical performance of the array-feed dielectric lens antenna was studied through electromagnetic simulations [7]. In the simulations, rectangular horn antennas were considered as elements of the array feed. By employing both a shaped dielectric lens and array feed, an almost flat aperture phase distribution was achieved. As a result, the radiated beam at the 30° direction could maintain the same beam shape at the 0° direction [7].

In this study, the realization of a shaped lens and array feed is pursued, and the appropriate simulation tool for this rather complicated configuration is identified. As an array element antenna, a patch antenna configuration is developed in place of the rectangular horn. In order to achieve proper excitation coefficients for the array feed, a power divider consisting of a microstrip circuit is designed. The shaped dielectric lens is fabricated by adequately forming a polycarbonate material. In order to confirm the design accuracies, electromagnetic simulation results and measured results are compared. As a simulator, the FEKO suite (ver. 5.3) is employed. The electric field distributions of the array feed and dielectric lens are obtained and achievement of design concepts is confirmed. Finally, the wide-angle beam scanning characteristics—radiation patterns and antenna gains—are confirmed. As a result, the realization of a wide-angle beam scanning antenna is confirmed.

## II. CONCEPT OF ARRAY-FEED SHAPED LENS ANTENNA

The antenna configuration is shown in Fig. 1. The dielectric lens antenna has an axisymmetrical structure around the Z axis. The lens surfaces were shaped based on Abbe's sine condition [4, 5]. Beam scanning is achieved by replacing the feed positions. The on-focus feed is placed at the origin of the XYZ axes. The off-focus feed for beam scanning is placed in the XZ plane. In the off-focus feed, a linear array antenna arranged in the Y axis direction is employed.

The roles of the lens antenna and the array feed cooperate in this configuration. The shaped lens antenna can achieve a constant wave front in the scanning plane. As a result, a sharp beam is obtained in the scanning plane. The array feed is designed to achieve a constant wave front in the transverse plane. Thus, a sharp beam is obtained in the transverse plane. With the assistance of these two parts, a sharp pencil beam is achieved in the wide-angle beam direction.

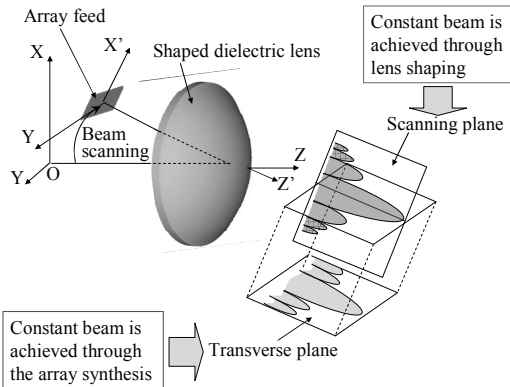


Fig. 1. Configuration of array feed and shaped lens antenna.

## III. DESIGN RESULTS OF THE ARRAY FEED LENS ANTENNA

### A. Shaped Dielectric Lens for Wide-Angle Scanning

The abilities of the shaped lens in 30° beam scanning are shown in Fig. 2. The effects of the lens are studied through ray tracings. The ideal condition is that all rays refracted by the lens become parallel. In the scanning directions of Fig. 2 (a), refracted rays become parallel and arranged in a straight line. However, in the transverse direction, refracted rays become curved and form a U-shaped line. The ray tracing results are converted to the antenna aperture phase distribution ( $\phi_{ap}$ ), as shown in Fig. 2 (b). In the

scanning plane, constant phases are achieved. However, in the transverse plane, large phase delays occurred. These phase delays produce radiation pattern degradation in the transverse plane. Thus, compensation of this phase delay is necessary to achieve excellent scanning characteristics. We employed an array feed configuration for this purpose.

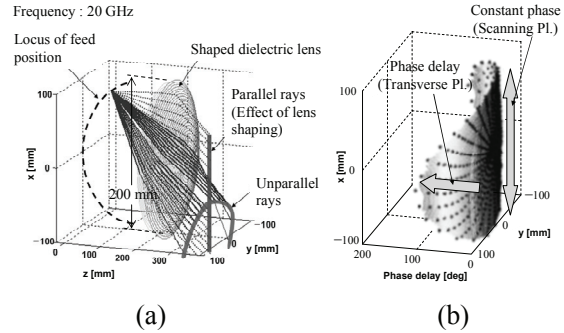


Fig. 2. Abilities of the shaped dielectric lens, (a) ray tracing result, and (b) aperture phase distribution ( $\phi_{ap}$ ).

### B. Array Feed

A configuration of the array feed is shown in Fig. 3. The array feed is directed to the lens direction, as indicated by the Z' axis. Array elements are arranged in the Y axis that correspond to the transverse direction. The radiation patterns of array elements in the scanning plane and the transverse plane are indicated by  $E_{ls}(\theta_s)$  and  $E_{lt}(\theta_t)$ , respectively.  $E_{ls}(\theta_s)$  has a rather narrow beam so as to illuminate the lens efficiently. Hence, the array element length in the X' axis direction is about 1.5 wavelengths. On the other hand,  $E_{lt}(\theta_t)$  has a wide beam width so as to ease the radiation pattern synthesis in the transverse plane. The array element length in the Y axis direction is 0.5 wavelengths. Array elements are excited with excitation coefficients  $V_i$ .

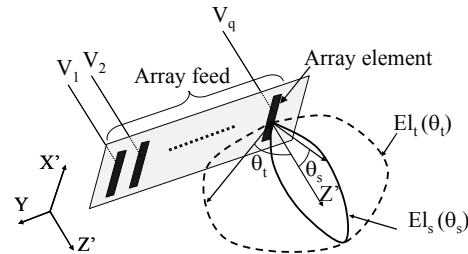


Fig. 3. Configuration of the array feed.

Figure 4 shows the geometry of the radiation pattern synthesis. L is the length between the lens and a feed horn. The array elements are located

along the Y axis.  $E_{lj}$  ( $j = 1, 2, \dots, q$ ) indicates array elements and  $y_j$  represents their positions.  $F(y_{Di})$  ( $i = 1, 2, \dots, p$ ) is objective radiation patterns on the lens surface that have  $p$  components, which are represented by Eq(1).

$$[F] = [B][V]. \quad (1)$$

Here,  $[F]$  components are expressed by complex numbers that have amplitude and phase values. Amplitude values are composed of the projected values of  $E_{ls}(\theta_s)$  in Fig. 7 (b) on the lens surface sampled at  $p$  points ( $y_{Di}$ ). Phase values are composed of  $p$  sampling points of the objective pattern of Fig. 6.  $[V]$  is excitation coefficients of array elements.  $[B]$  is a  $p \times q$  matrix which expresses contributions of  $[V]$  to each lens position of  $y_{Di}$  ( $i=1, 2, \dots, p$ ).

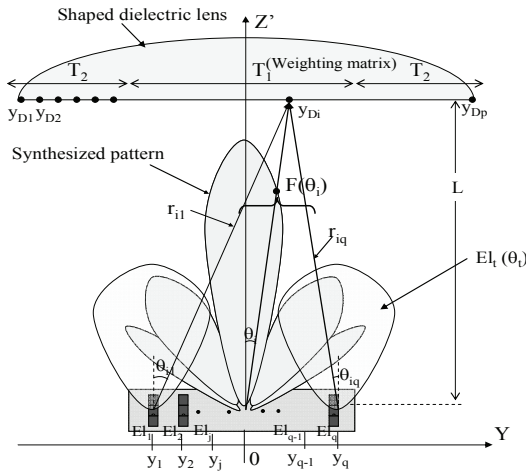


Fig. 4. Geometry of radiation pattern synthesis.

Equation (1) can be solved using the Leased Mean Square method.  $[V]$  is expressed by the next equation [8].

$$[V] = ([B]^H [T]^H [T] [B])^{-1} [B]^H [T]^H [T] [F]. \quad (2)$$

Here,  $H$  indicates complex conjugate and transpose of a matrix.  $[T]$  is a weighting matrix used to emphasize certain angular regions.  $[T]$  has only diagonal components ( $t_{ii}$ ). By imposing large weights on the lens region, both amplitude and phase radiation patterns are designed adequately. The most suitable value of  $[T]$  is determined by trial and error [6].

Excitation coefficients ( $V_i$ ) of Eq.(2) are shown in Figs. 5 (a) and (b). Eight array elements are employed. As for the array element, a rectangular aperture of  $1.5 \times 0.5$  wavelengths is considered. The radiation patterns ( $E_{ls}(\theta_s)$  and  $E_{li}(\theta_i)$ ) are expressed by the following equation.

$$E(\theta_s, \theta_t) = \frac{j e^{-jkR}}{\lambda R} \frac{\sin(ku1.5\lambda/2)}{(ku1.5\lambda/2)} \frac{\sin(kv0.5\lambda/2)}{(kv0.5\lambda/2)}. \quad (3)$$

$$u = \sin \theta_s \cos \theta_t, \quad v = \sin \theta_s \sin \theta_t$$

In Fig. 5 (a), amplitude taper is formed to the edge elements. In Fig. 5 (b), large phase delay is formed to the edge elements. By applying  $V_i$  to Eq.(1), the radiated electric fields (amplitude and phase) of the array feed are calculated. These radiated electric fields are refracted by the lens and perform the antenna aperture distribution. The calculated antenna aperture phase distributions are shown in Fig. 6. The data in Fig. 6 corresponds to that of Fig. 2 (b). The objective pattern indicates the opposite phase ( $-\phi_{ap}$ ) of Fig. 2 (b). It is recognized that excellent  $-\phi_{ap}$  is achieved in the designed pattern. Thus, it is certain that sufficient phase delay compensation can be achieved using the array feed.

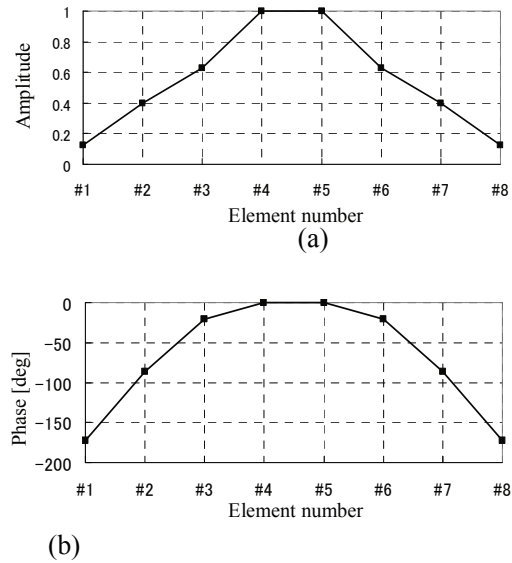


Fig. 5. Excitation coefficients ( $V$ ) for  $30^\circ$  beam scanning, (a) amplitude of  $V$ , and (b) phase of  $V$ .

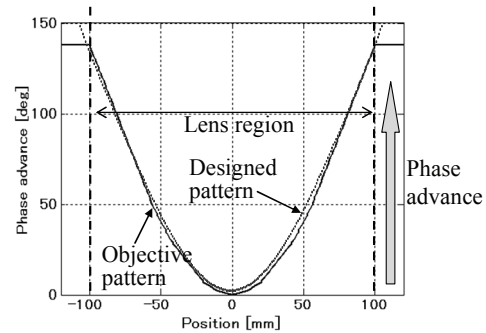


Fig. 6. Aperture phase distribution from array feed ( $-\phi_{ap}$ ).

## IV. SIMULATION OF THE ARRAY FEED LENS ANTENNA

### A. Simulation Condition

The simulation methods and simulation details are summarized in Table 1. It is assumed that a very large memory is needed for calculation of the array feed and the dielectric lens. Utilization of the MLFMM becomes inevitable. In order to apply MLFMM, the surface equivalent principle is employed for the dielectric substrate of the array feed and the dielectric lens body. Mesh sizes and the number of meshes in the simulation objects are given in Table 1. More than 10,000 meshes are used in simulating each object. The total memory size of 5.1 GB and the calculation time of 20 hours are required.

Table 1: Simulation parameters.

Computer specification		CPU	Xeon 3.2 GHz × 2	
		Software	FEKO (Suite 5.3) with MLFMM	
Frequency		20 GHz		
Simulation models of dielectric material		Surface equivalence principle (SEP)		
Array feed	Dielectric substrate	Finite plane		
		Mesh size	$\lambda/20$	
	Patch	Mesh size	Edge	$\lambda/40$
		Face	$\lambda/20$	
Number of meshes		25,086		
Shaped dielectric lens	Mesh size		$\lambda/3.5$	
	Number of meshes		17,068	
Used memory		5.1 GBytes		
Calculation time		20 H		

### B. Simulation Results of the Array Element

The actual structure of the fabricated array element is shown in Fig. 7 (a). The array element is composed of three square patch antennas [7]. The center patch is fed by the feed pin. Square patches are connected by thin connecting lines in order to be excited in phase. All the metallic parts are conformed on the dielectric substrate of  $\epsilon_r = 2.2$ .

The square patch size becomes the half wavelength in the dielectric substrate. The connecting line length is determined so as to excite three patches in phase. Simulated results are shown in Fig. 7(b). In the  $El_s(\theta_s)$ , a rather sharp beam antenna is achieved. The edge level becomes less than -15 dB. In the  $El_t(\theta_t)$  plane, the broad beam is achieved.

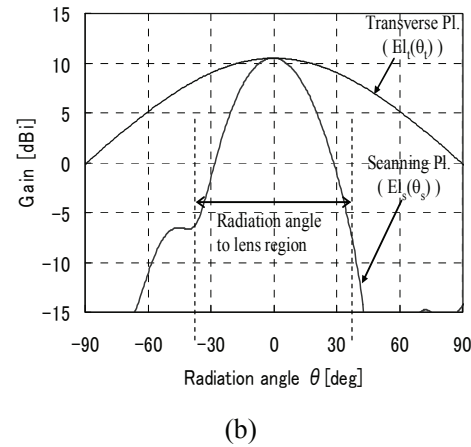
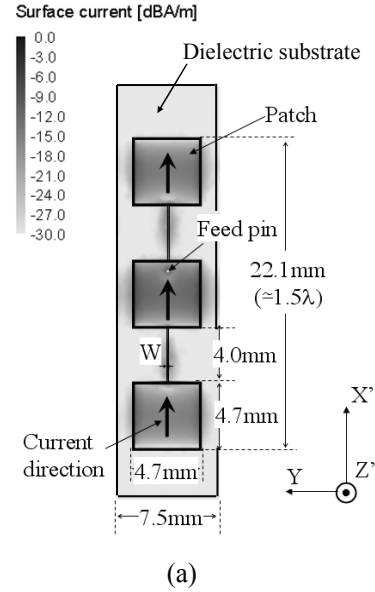


Fig. 7. Configuration of array element, (a) structure, and (b) radiation pattern.

### C. Simulation Results of the Array Feed

Electrical field distributions of the array feed are shown in Fig. 8. In the scanning plane of Fig. 8 (a), many curved regions are observed. These regions correspond to wave fronts. It is recognized that wave fronts coincide with the spherical wave fronts. Thus, in the scanning plane, spherical waves are produced. In the transverse plane of Fig. 8 (b), the synthesized wave front becomes flatter than the spherical wave front. This wave front change is considered the result of the phase advance. Consequently, it is anticipated through this wave front shape that the phase advance design has been successfully achieved.

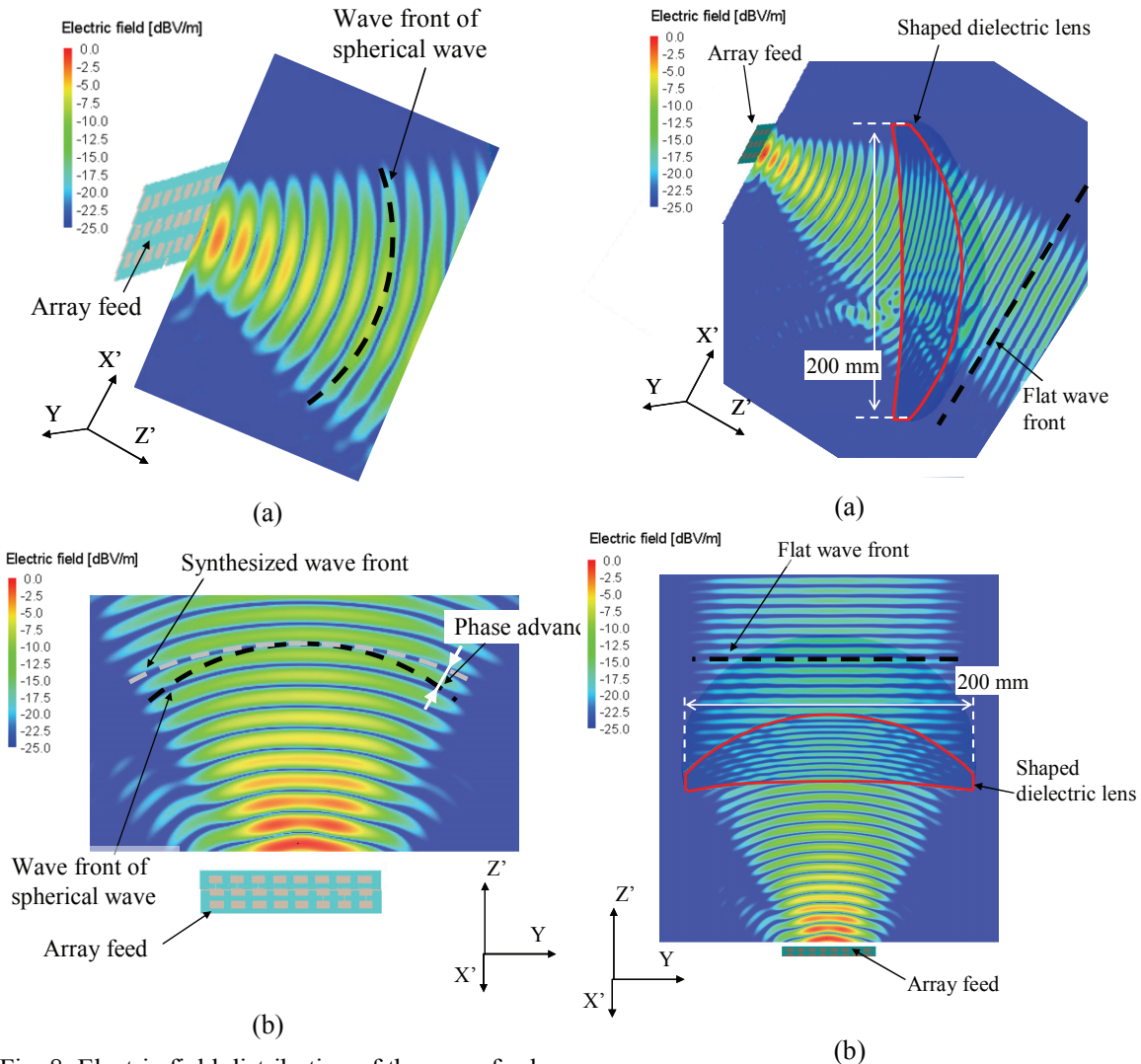


Fig. 8. Electric field distribution of the array feed, (a) scanning plane, and (b) transverse plane.

Fig. 9. Electric field distribution of 30° scanning beam, (a) scanning plane, and (b) transverse plane.

**D. Simulation Results of Array and Shaped Lens Antenna**

Electrical field distributions of the dielectric lens are shown in Fig. 9. In the scanning plane of Fig. 9 (a), it is recognized that the flat wave front is achieved in front of the lens. In the transverse plane of Fig. 9 (b), the flat wave front is also achieved. Consequently, desired constant phase distributions are expected in the antenna aperture plane.

Antenna aperture distributions are shown in Fig. 10. In the illumination distribution of Fig. 10 (a), the high intensity region is shifted to the upper part of the aperture plane. This reason is clearly recognized from the electrical field distribution of Fig. 9 (a). Electrical fields on the lower part of the antenna aperture become weak. In order to achieve symmetrical illumination distribution,

the tilt angle of the array feed should be larger than 30°. In the phase distribution of Fig.10 (b), excellent constant phase characteristic is achieved. The effects of dielectric lens shaping and the array feed are confirmed.

**E. Radiation Pattern**

Radiation beam shapes are shown in Fig. 11. In the bore site beam of Fig. 11 (a), an axisymmetrical beam shape is achieved. In this case, two array elements are arranged side by side, as shown in Fig. 14 (b). Three dB beam widths in the scanning ( $\theta$ ) and transverse ( $\phi$ ) planes both become 4.5°. In the 30° scanning beam of Fig. 11 (b), an almost axisymmetrical beam is achieved. Three dB beam widths in the scanning and transverse plane become 4.5° and

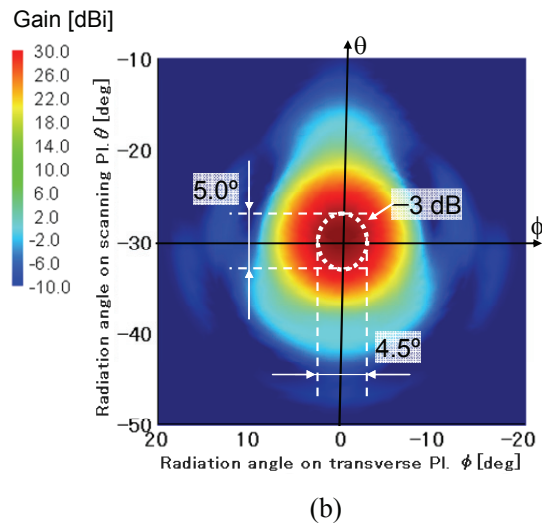
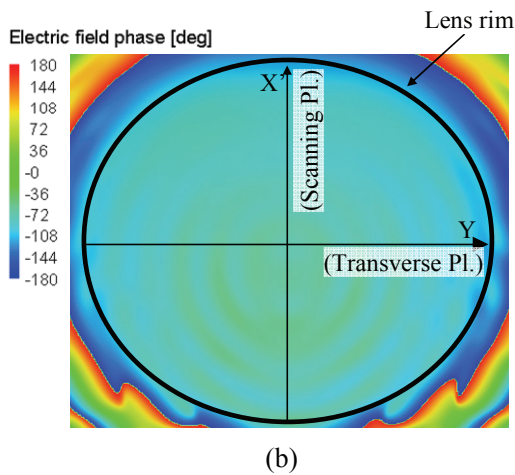
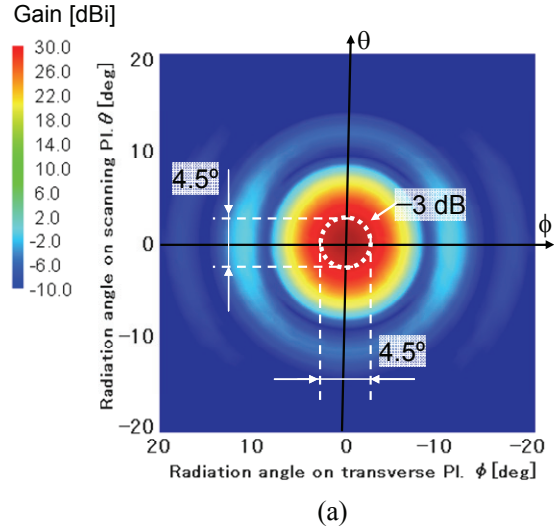
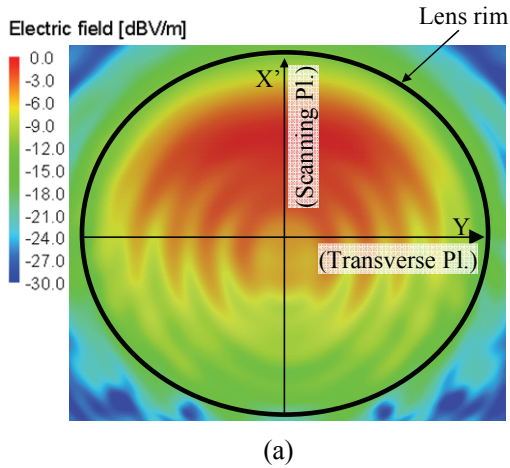


Fig. 10. Aperture distribution of 30° scanning beam, (a) field intensity, and (b) phase.

5.0°, respectively. The reason for the broadened beam width of 5.0° on the scanning plane is recognized from the intensity distribution on the scanning of Fig. 10 (a).

**V. MEASURED RESULTS**

**A. Measurement Setting**

Measurement set up of the radiation patterns is shown in Fig. 12. The off-focus feed is placed at 30° offset from the dielectric lens axis (Z). The feed position adjustment is very important. The alignment accuracy of about 1 mm is achieved. During the measurements, the supporting metal frames and the antenna back area are covered by the electromagnetic absorbing sheet. Measured planes include the scanning and the transverse planes, as shown in Fig. 12. The dielectric lens antenna is composed of the polycarbonate whose electric constants are  $\epsilon_r = 2.64$  and  $\tan\delta = 0.0075$ .

Fig. 11. 2D radiation beam shapes of the bore site and 30° scanning beams, (a) bore site beam, and (b) 30° scanning beam.

The antenna diameter is 200 mm and thickness is 57 mm. The antenna weight is 1.3 Kg.

**B. Array feed**

First of all, the fabricated array element is shown in Fig. 13 (a). Three square patches are excited in phase through connecting lines. Measured and simulated radiation patterns are shown in Fig. 13 (b). In  $E_{\theta_s}(\theta_s)$  and  $E_{\theta_t}(\theta_t)$  patterns, simulated and measured results agree very well. Thus, it is shown that the fabrication of the array element has been successfully performed. The band width characteristics of the array feed is determined by the input impedance

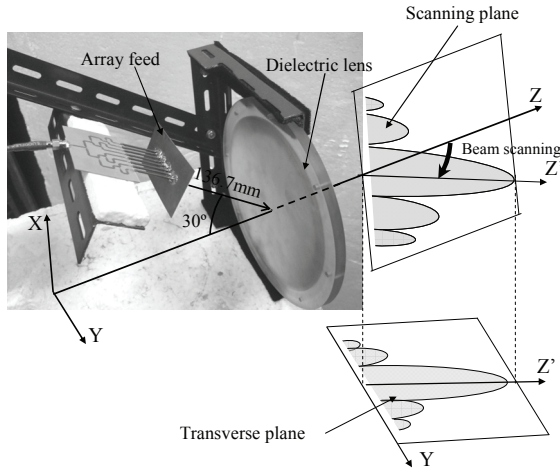


Fig. 12. Antenna structure for radiation pattern measurement.

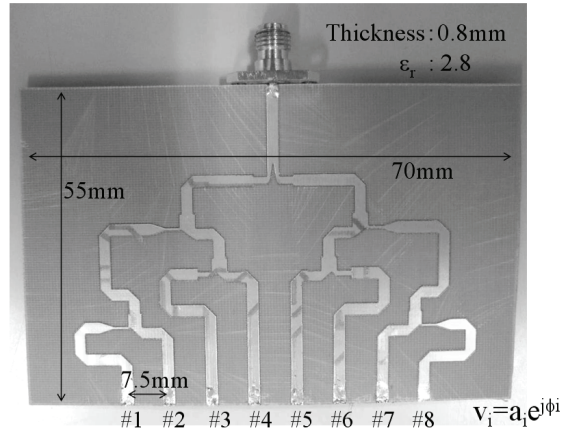


Fig. 15. Power divider for the 30° scanning beam.

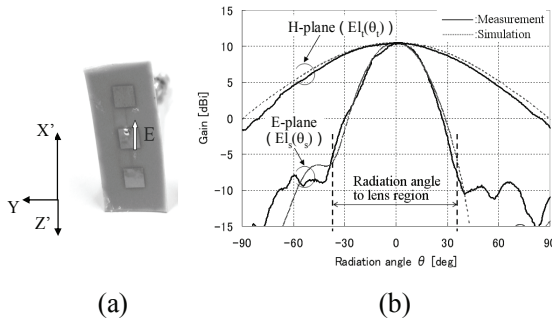


Fig. 13. Array element, (a) fabricated, and (b) radiation pattern.

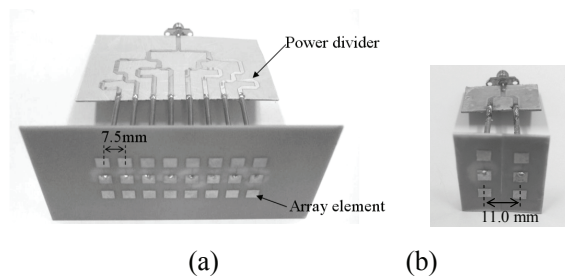


Fig. 14. Array feed, (a) 30° scanning beam, and (b) Bore site beam.

bandwidth of the patch antenna [9]. About 20% bandwidth in  $VSWR < 2$  was reported.

Next, configurations of array feed are shown in Fig. 14. The array feed for a 30° scanning beam, as shown in Fig. 14 (a), is composed of eight array elements.

The array feed for the bore site is composed of two array elements. In this feed, an almost axisymmetrical beam is achieved. Array elements of both the array feeds are excited through the power divider.

### C. Power Divider

Configuration of the power divider for the 30° scanning beam is shown in Fig. 15. Branching circuits are composed on the dielectric substrate of  $\epsilon_r = 2.8$  and  $\tan\delta = 0.0018$ . The circuit line lengths determine the phase values of terminals. The circuit line widths at the branching points determine the dividing power values of the terminals. As the result, excitation coefficients ( $V_i$ ) are designed. In order to confirm the achievement of this power divider, measured amplitude and phase characteristics of all terminals are obtained.

Measured frequency characteristics are shown in Figs. 16 (a) and (b). At the amplitude characteristics of Fig. 16 (a), frequency dependences are divided into two groups. The first one consists of terminals  $a_2, a_7$  and  $a_1, a_8$ . The other group consists of terminals  $a_3, a_6$  and  $a_4, a_5$ . Within each group, frequency dependence becomes similar. However, frequency dependence becomes opposite between different groups. Hence, at the branching point dividing #1,#2 terminals and #3,#4 terminals, opposite frequency dependence is produced. By refining these branching points, all the curves can become parallel. The insertion loss of this power divide can be estimated by summing up the square values of  $a_i$ . The estimated insertion loss is about 6.5 dB. The insertion loss is divided into the strip line loss of 2 dB and radiation loss of 4.5 dB. Because the purpose of this paper is to achieve the accurate excitation coefficient, reduction of this large insertion loss is considered as the future subject. At the phase characteristics of Fig. 16 (b), frequency dependences become almost similar in all terminals. At 20 GHz points, measured and design objects agree very well.

Excitation coefficients of the power divider are summarized in Fig.17. The target values are the designed results of Fig.5. In the amplitude and phase characteristics, target values are accurately achieved with the fabricated power divider.

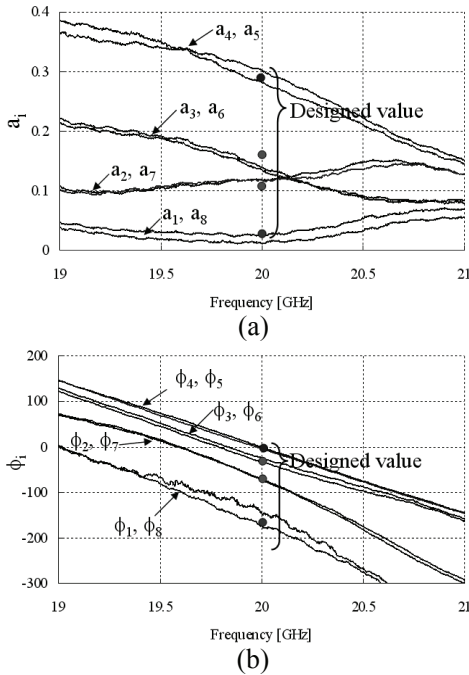


Fig. 16. Amplitude and phase characteristics of the power divider, (a) amplitude, and (b) phase.

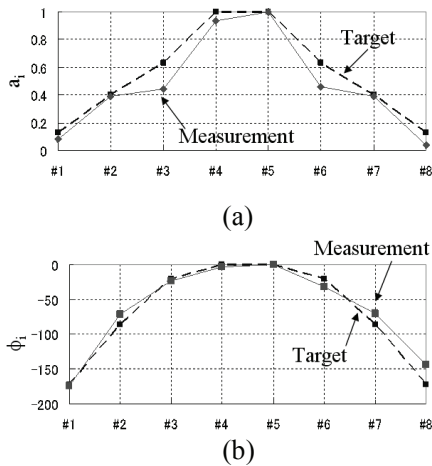


Fig. 17. Excitation coefficients, (a) amplitude of V, and (b) phase of V.

**D. Radiation Pattern**

Measured and simulated beam scanning characteristics are shown in Fig.18. In the scanning plane of Fig.18 (a), measured and simulated results agree very well. The beam width in the 30° scanning beam becomes slightly broader than the bore site beam. This result is

anticipated from the beam shape of Fig.11 (b). The antenna gain decrease at the 30° scanning angle is 1.7 dB. A rather small gain decrease is achieved. In the transverse plane of Fig.18 (b), measured and simulated results agree very well. Almost identical beam widths are achieved in the bore site and at the 30° scanning beams. As a result, realization of the wide-angle beam scanning antenna is confirmed.

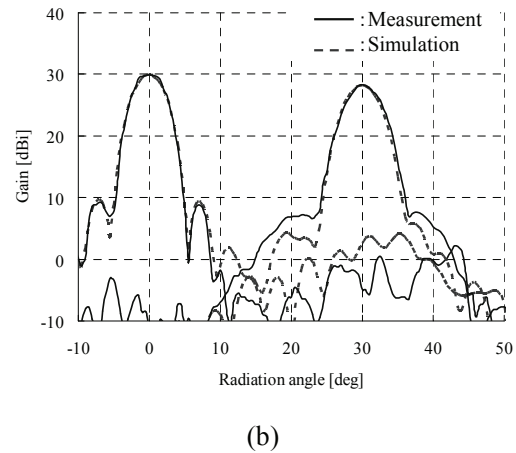
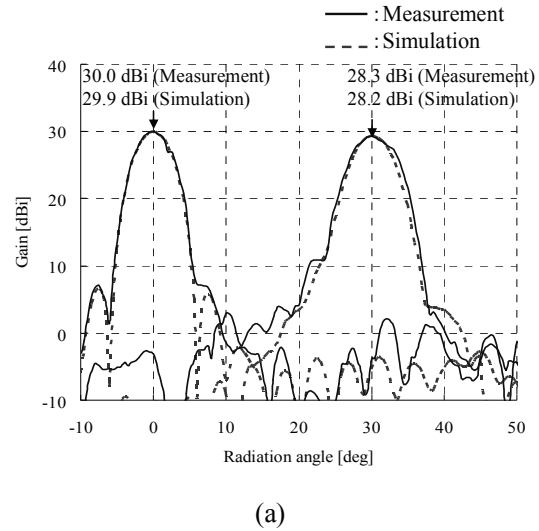


Fig. 18. Radiation patterns of the array feed lens antenna, (a) scanning plane, and (b) transverse plane.

In order to confirm the antenna gain, antenna measurement is conducted. The configuration of the gain reference antenna is shown in Fig.19. In this case, as the gain reference, a half wave dipole antenna is attached at the #5 output terminal. The others are terminated by 50 Ω resistances. The power ratio of each port

Table 2: Power ration of power divider.

Port number	#1	#2	#3	#4	#5	#6	#7	#8
Power ratio	0.002	0.059	0.076	0.347	0.384	0.082	0.059	0.001

obtained from Fig. 17 is shown in Table 2. The power ratio of the #5 port becomes 0.384. The purpose of this configuration is to avoid the affect of large insertion loss of the power divider.

The radiation patterns of the gain reference antenna and 30° scanning beams are shown in Fig. 20. These values are measured using radiation power. At the gain reference antenna, a measured power of -68.0 dBm is obtained, which corresponds to -2.0 dBi by the following equation.

$$\begin{aligned}
 -68.0 \text{ [dBm]} &= 2.15 \text{ [dBi]} \times 0.384 \\
 &= -2.0 \text{ [dBi]} \quad (4)
 \end{aligned}$$

The measured power of the 30° scanning beams becomes -37.7 dBm. Thus, the antenna gain is estimated to be 28.3 dBi, as shown in Fig. 20. This value is consistent with the simulated value of 28.2 dBi.

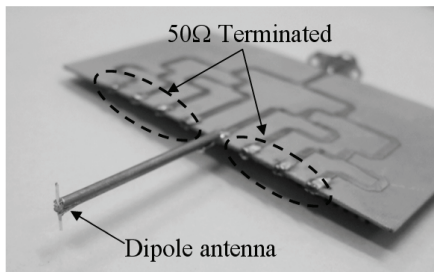


Fig. 19. Structure of gain reference antenna of the off-focus feed.

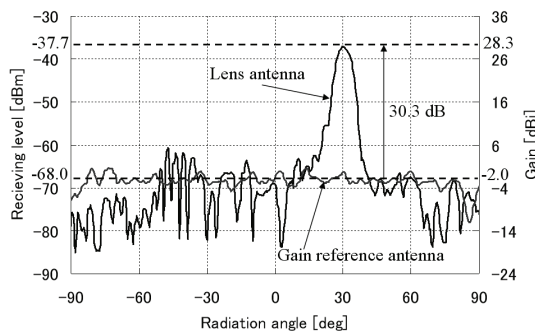


Fig. 20. Gain calculation from measurement.

The measured gain of the bore site beam is obtained through the same method. In this case, the dipole antenna is attached at the one terminal of Fig. 14 (b) and the other is terminated by 50 Ω resistance. The measured and simulated gains of the bore site beam also agree very well, as shown in Fig. 18 (a). In conclusion, this study has ensured that antenna gains can be successfully achieved.

### VI. CONCLUSIONS

Realization of the shaped dielectric lens antenna with array feed is ensured through measurement and electromagnetic simulations. Important technical results developed are summarized as follows.

- (1) As an array element, a convenient patch antenna configuration is developed that replaces the previous rectangular horn antenna.
- (2) For the 30° beam scanning, an eight-branch power divider is fabricated. Accurate excitation coefficients are confirmed through the measured results.
- (3) The achievements of design concepts of the array feed and the shaped lens are confirmed through electromagnetic simulations of the electric field distributions.
- (4) Antenna radiation characteristics at 30° beam scanning are ensured through the radiation pattern measurements. Beam shapes that are almost identical to the on-focus feed are confirmed.
- (5) Excellent antenna gains coinciding with simulated values are ensured through measurement.

### REFERENCES

- [1] Research and Innovative Technology Administration, <http://www.its.dot.gov/index.htm>.
- [2] Japanese Ministry of Land, Infrastructure, Transport and Tourism, Road Bureau ITS Homepage, <http://www.mlit.go.jp/road/ITS/>.
- [3] T. Kato, T. Tanizaki, T. Ishii, H. Tanaka, and Y. Takimoto, “76 GHz high preference radar sensor featuring fine stem scanning mechanism utilizing NRD technology,”

*IEEE Intelligent Vehicles Symposium*, pp. 163-170, May 2001.

- [4] Y. T. Lo and S. W. Lee, *Antenna Handbook*, Van Nostrand Reinhold Company, vol. 2, pp. 16-23, 1988.
- [5] Y. Tajima and Y. Yamada, "Design of Shaped Dielectric Lens Antenna for Wide Angle Beam Steering," *Electron. and Comm. in Japan Part III*, vol. 89, no.2, pp. 1-12, February 2006.
- [6] Y. Tajima and Y. Yamada, "Improvement of Beam Scanning Characteristics of a Dielectric Lens Antenna by Array Feed," *IEICE Trans. Fundamentals*, vol. E91-A, no. 7, pp. 1616-1624, July 2008.
- [7] Y. Tajima, N. Michishita and Y. Yamada, "FEKO Simulation of the Shaped Dielectric Lens Antenna Capable of Wide Angle Beam Scanning," *25<sup>th</sup> International Review of Progress in Applied Computational Electromagnetics*, March 2009.
- [8] S. Takubo and Y. Yamada, "Low Sidelobe and Asymmetrical Pattern Synthesis of an Unequally Spaced Array Antenna," *IEICE ISAP'00*, vol. 3, pp. 1195-1198, Aug. 2000.
- [9] Y. Tajima and Y. Yamada, "Design of a Patch Array Feed for the Dielectric Lens Antenna Achieving Wide Angle Beam Scanning," *IEEE International Conference on Communication Systems*, p. 46, Nov. 2008.



**Yosuke Tajima** received the B.S., M.S. and Dr. degrees in Electronics Engineering from National Defense Academy, Kanagawa, in 2000, 2005 and 2009. He enlisted in Japan Air Self Defense Force in 2000. He was engaged in tests and developments of radar and avionics equipments. His current research interests include lens and phased array antennas. Now he is a Captain.



**Shinji Kamada** graduated from Akita University and received the B.S. degree in Electrical and Electronic Engineering in 2004. He enlisted in Japan-Air-Self-Defense-Force in 2004. Now he is a technical official. He was engaged in tests of electronic equipments. He entered the Master course of

Electrical and Electronic Engineering of National Defense Academy in 2008. His current research interests include lens antennas and metamaterial antennas.



**Naobumi Michishita** received the B.E., M.E., and D.E. degrees in Electrical and Computer Engineering from Yokohama National University in 1999, 2001, and 2004, respectively. He joined the Department of Electrical and Electronic Engineering, National Defense Academy, as a research associate in 2004. He was a visiting scholar at the University of California, Los Angeles from 2006 to 2007. He received the Young Engineer Award from the IEEE AP-S Japan Chapter and IEICE in 2004 and 2005, respectively. His current research interests include metamaterial antennas and electromagnetic analysis. He is a member of IEEE.

**Yoshihide Yamada** graduated from the Nagoya Institute of Technology and received the BS and MS degrees in electronics in 1971 and 1973, respectively. He received the DE degree from the Tokyo Institute of Technology in 1989. In 1973, he joined the Electrical Communication Laboratories of the Nippon Telegraph and Telephone Corporation (NTT). Until 1984, he was engaged in research and development related to reflector antennas for terrestrial and satellite communications. Beginning in 1985, he engaged in R&D for base station antennas for mobile radio systems. In 1993, he moved to the NTT Mobile Communications Network Inc. (NTT DoCoMo). In 1995, he was temporarily transferred to the YRP Mobile Telecommunications Key Technology Research Laboratories Co., Ltd. At the same time, he was a guest professor at the cooperative research center of Niigata University, and a lecturer at the Science University of Tokyo, both from 1996. In 1998, he took a position as a professor at the National Defense Academy. At present, he is interested in very small RFID antennas, shaped dielectric lens antennas, and electromagnetic simulations of large objects. He is a member of the IEICE and JSST of Japan and an IEEE society member of AP, VT, and COMM.